Quadruplex Slot Antenna for Dual-standard Operation with Small Frequency Ratio

Jianfeng Qian, Benito Sanz Izquierdo, Steven Gao, *Fellow, IEEE*, Hanyang Wang, *Fellow*, *IEEE*, Hai Zhou, and Huiliang Xu

***Abstract*—In this communication, a novel four-port slot antenna designed for both 5G New Radio (NR) and WiFi operations is introduced. Wideband NR antennas are achieved using a hybrid mode concept. Then, two NR slot antennas are co-designed as a radiative bandstop structure. By moving the resonance frequencies of the hybrid modes close to the band-reject points of this bandstop filter, a wideband decoupled dual-antenna structure is achieved. To enhance functionality, two additional ports are incorporated into the dummy slot area between these two NR ports, resulting in a quadruplex antenna. In this final configuration, two of the antennas are optimized for 5G NR applications, covering the 5G N77, N78, and N79 bands (3.3 GHz-5.0 GHz), while the remaining two antennas serve the WiFi band (5.15 GHz-5.8 GHz). Compared to other presented works, the simulation and experimental results demonstrate that this work not only, for the first time, achieves simultaneously wideband in-band and small frequency ratio (1.05) out-of-band duplex in one single module, but also has the advantages of high isolation, compact size, and low cost.**

[1] ***Index Terms*—Antenna isolation, duplex, multiple-input–multiple-output, quadruplex, slot antenna, wideband.**

I. INTRODUCTION

OVER the past century, there has been significant progress in the field of wireless communication technology. The limited space available within terminal devices has created a demand for compact antenna solutions that can meet the requirements of multiple communication standards, such as 4G LTE, WiFi, GNSS, and Bluetooth while ensuring low mutual coupling among the antennas. Thus, the development of compact antenna solutions would greatly enhance the versatility and functionality of terminal products.

To address the mutual coupling problem, many technologies can be found in the literature such as decoupling networks [1, 2], parasitic elements [3, 4], neutralization lines [5], surface wave suppression [6, 7], and deliberately designed antenna arrangements [8, 9]. Unfortunately, most of these techniques are only verified with narrow-band antennas, which may only be effective for some narrow-band applications such as Bluetooth and 2.4GHz WiFi.

It is widely recognized that duplex/multiplex antennas offer a feasible solution to minimize the antenna volume. Such antennas enable the concurrent operation of multiple antennas within a compact structure, where different antennas can be co-designed and decoupled on the antenna side. While numerous studies have been conducted on in-band duplex/multiplex antennas [10-18], relatively few have explored the challenges posed by out-of-band duplex/multiplex scenarios, particularly in the context of closely spaced passbands. Some out-of-band duplex (OBD) works either suffer from big frequency ratios [19-24] or limited bandwidths [23, 24]. As such, there remains a pressing need for multiplex antenna technology that can effectively address both wideband in-band and small frequency ratio out-of-band problems.

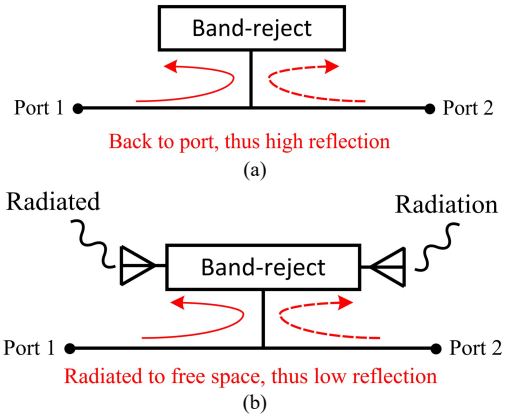

Fig. 1. Conceptual illustration of the proposed self-decoupled antennas. (a) Conventional bandstop network. (b) Proposed decoupled slot antennas using radiative bandstop concept.

This paper introduces a quadruplex slot antenna that addresses both in-band duplex (IBD) and out-of-band duplex (OBD) problems within a single module. The study reveals that two isolated slot antennas, sharing a common radiator, can be achieved by configuring them to form a radiative bandstop filtering structure, as depicted in Fig. 1. With this structural arrangement, when one port is activated, mutual coupled energy is reflected, preventing the transfer of energy into another port and resulting in low mutual coupling. Furthermore, the reflected energy is radiated, ensuring low reflection coefficients for both antenna ports, thereby facilitating duplex operation. Subsequently, the bandwidth of the single-mode duplex antenna is enhanced by incorporating higher-order modes to cover NR bands. The distinct current distributions for these modes create a dummy current area between two NR antennas, where two additional WiFi antenna ports are designed. This leads to the realization of a four-port antenna. Notably, the frequency ratio between the upper edge of the NR band and the lower edge of the WiFi band is only 1.03. Section III-B introduces the methods employed to decouple these closely arranged operating bands. In the final implementation, all antennas are effectively decoupled and isolated, achieving a minimum isolation of 19 dB.

II. RESONATOR-LOADING SLOT ANTENNAS

A. 2-Element MIMO Slot Antenna

First, the mechanism of the proposed duplex technique is explained with the fundamental structure in Fig. 2, in which two identical slot antennas are connected together, sharing the same ground plane. It is

This work was supported by Huawei Technology Ltd., and the EPSRC grant (EP/S005625/1) and the Royal Society - International Exchanges 2019 Cost Share (NSFC) (IEC\NSFC\191780). (Corresponding author: Jianfeng Qian.)

J. F. Qian and Benito Sanz Izquierdo are with the University of Kent, Canterbury CT2 7NT, U.K. (e-mail: jq42@kent.ac.uk).

S. Gao is with the Chinese University of Hong Kong, Hong Kong.

H. Zhou, H. Xu, and H. Wang are with Huawei Technology Ltd.

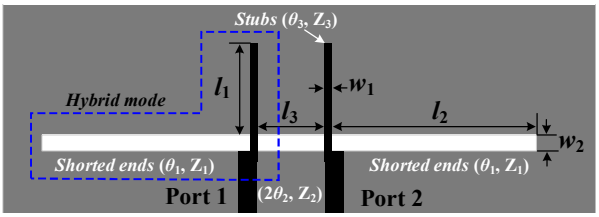

Fig. 2. Structure of the dual-antenna module. Dimensions in mm: l_1 = 5.85, l_2 = 29.15, l_3 = 14.9, w_1 = 0.7, w_2 = 3.

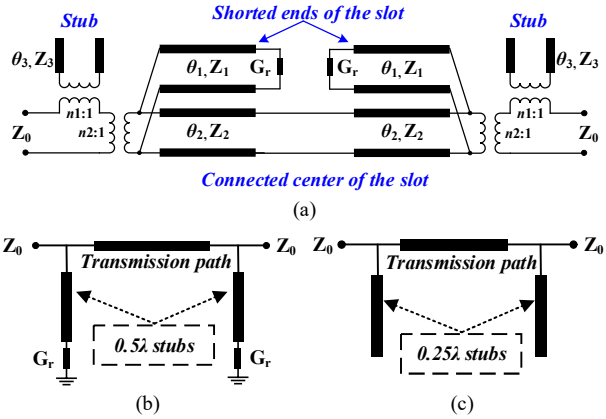

Fig. 3. (a)Transmission line model for the dual-antenna module. (b) Simplified conceptual model of the antenna module which shows radiative bandstop response. (c) transmission line mode for a 3rd order bandstop filter.

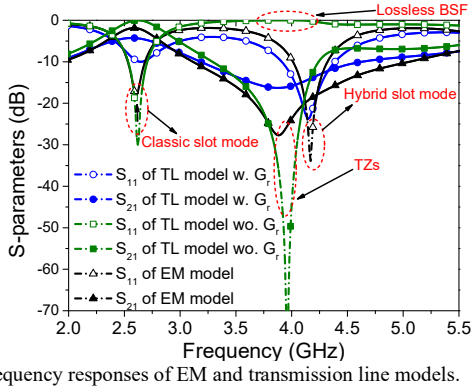

Fig. 4. Frequency responses of EM and transmission line models.

found through our study that such architecture ensures two inherently isolated channels when the slot is operating over a microstrip-line-to-slot hybrid mode (MSHM).

An equivalent circuit model of the dual-antenna module is shown in Fig. 3(a). The model contains transmission lines that are characterized by their electrical lengths and characteristic impedance at the resonant frequency of the fundamental slot mode (f_0). The microstrip-slotline transition is modeled using ideal transformers with tuning ratios of $n1$ and $n2$, which are set to be unity for simplicity. The slot is represented by short-circuited ideal transmission lines (θ_1, θ_2) with a terminal radiation conductance G_r that denotes the radiated power from the slot. As the slot is fed off-center and the longer portion (θ_1) contributes the most to the radiation, the radiation resistance of the short portion (θ_2) is neglected for simplicity.

This model can be simplified into a transmission path with two open-ended stubs, as shown in Fig. 3(b). Fig. 3(c) shows a transmission line model of a 3rd-order band-stop filter [25]. When the length of the stub in Fig. 3 (c) is a quarter wavelength at the centre frequency of the stopband, the virtual-short point blocks the transmission between two ports. Comparing the structure in Fig. 3(b) to (c), we can notice that the dual-antenna module is a lossy bandstop filter at the frequency where the length of θ_1 is about half-wavelength. With the transformation of a quarter-wavelength, the short ends of the

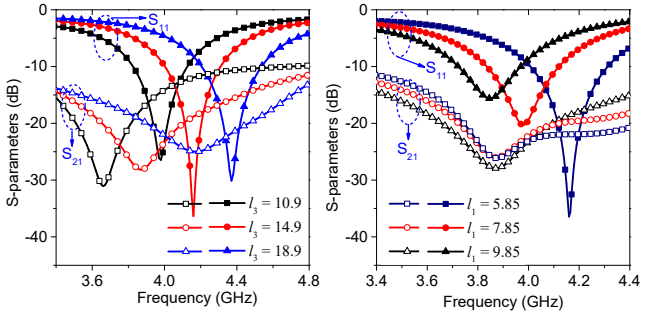

Fig. 5. Parametric studies with different feeding dimensions. (a) Feeding position. (b) Feedline lengths.

slot will be inverted to open ends just like the structure of the bandstop filter in Fig. 3(c).

In a conventional bandstop network, as depicted in Fig. 3(c), the signal is reflected back to the input port within its stopband, resulting in a high reflection coefficient, as shown in Fig. 1 (a). However, due to the radiating characteristics of the slot structure, the radiation resistance in Fig. 3(b) absorbs the reflected energy, leading to a low reflection coefficient as illustrated in Fig. 1(b). Consequently, the proposed hybrid mode exhibits a bandstop-radiative response near its resonance frequency.

The responses for both transmission line and EM models are plotted and compared in Fig. 4 with the following initial circuit parameters: Z_0 = 50 Ohm, $Z_1 = Z_2$ = 187 Ohm, Z_3 = 123 Ohm, G_r = 0.023 S, θ_1 = 150°, θ_2 = 30°, θ_3 = 63°. The electric properties of the element in the model are set at 3.3GHz. There are two resonances arise for each model. The first resonance is the classical slot mode. For this slot mode, the structure behaves like a bandpass filter with very high mutual coupling.

However, for the hybrid mode, which emerges at approximately 4.2 GHz, the entire structure functions as a dispersive bandstop filter (BSF) [25]. In a non-radiative BSF with G_r set to zero, the energy is reflected back to the input port within the stopband, resulting in an all-reflective S_{11}, as depicted in Fig. 4 (green lines with square symbols). In contrast, the proposed radiative slot structure allows the energy in the stopband, which would typically be reflected back to the port, to be radiated. Consequently, a low reflection coefficient is achieved. Furthermore, a transmission zero (TZ) slightly lower than the center frequency of the antenna's operating band arises for both electromagnetic (EM) and transmission line models.

Parametric studies on different feeding positions and feedline lengths were carried out as illustrated in Fig. 5. The other dimensions are kept unchanged as Fig. 2. First, the feed position, which governs the length of θ_1 in Fig. 3(a), influences both the operating band of the hybrid mode and the location of the transmission zero (TZ), as depicted in Fig. 5 (a). As the feed position of two ports moving away from each other, both the locations of the hybrid mode and TZ are shifted to lower frequency band. According to the analysis above, the arisen of the TZ is contributed to the bandstop structure, whose location is dominated by the length of θ_1. The resonance frequency of the hybrid mode is decided by the interaction of microstrip line and slotline, as illustrated in Fig. 2. When the feed position is changed, the length of θ_1 is altered. Consequently, the position of the feed controls both the resonance frequency of the hybrid mode and the location of the TZ.

The length of the feedline stub (l_1 in Fig. 2, θ_3 in Fig. 3(a)) can be utilized to shift the resonance frequency of the hybrid mode closer to the TZ, resulting in higher isolation, as shown in Fig. 5(b). When the stub length is increased, the resonance frequency of the hybrid mode shifts to lower frequency while the position of the TZ keeps unchanged.

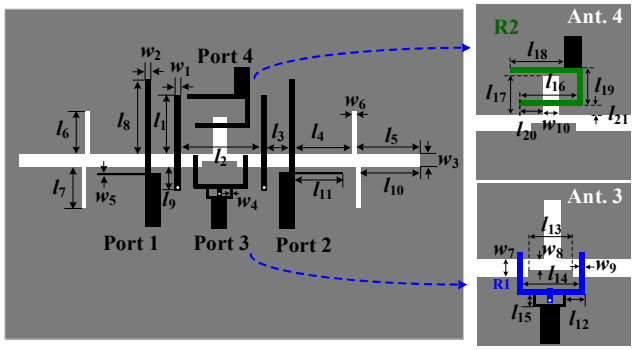

Fig. 6. Geometry of the quadruplex antenna. Dimensions in mm: l_1= 6.1, l_2= 14.8, l_3= 2.5, l_4= 14.98, l_5= 13.28, l_6= 9.8, l_7= 13.3, l_8= 5.95, l_9= 4.8, l_{10}= 14.78, l_{11}= 8.3, w_1= 1, w_2= 0.5, w_3= 3, w_4= 0.2, w_5= 0.15, w_6= 1.25, l_{12}= 3.5, l_{13}= 10, l_{14}= 7.8, l_{15}= 2.6, l_{16}= 5.7, l_{17}= 10.35, l_{18}= 9.7, l_{19}= 2, l_{20}= 2.8, l_{21}= 8.95, w_7= 3.3, w_8= 1.65, w_9= 0.8, w_{10}= 3.

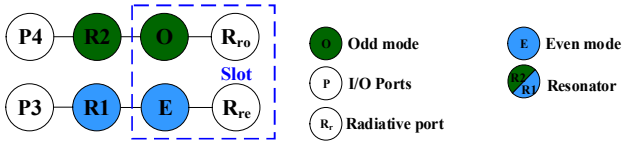

Fig. 7. Coupling topologies for the WiFi antennas.

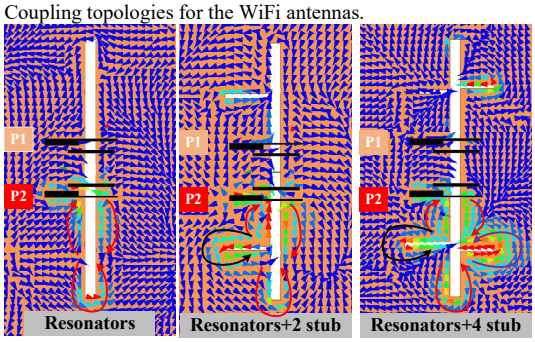

(a) (b) (c)

Fig. 8. Evolution of the wideband slot antennas. (a) reference design 1 with current vector plot at 4.2 GHz, (b) reference design 2 with current vector plot at 4.5 GHz, (c) reference design 3 with current vector plot at 5 GHz.

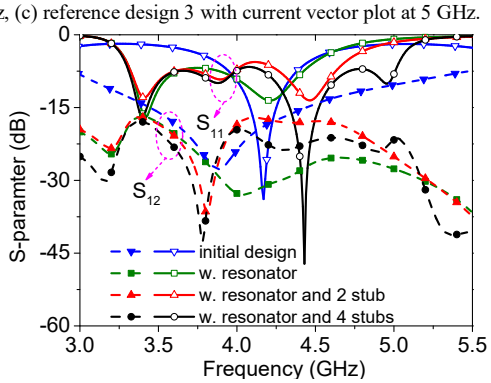

Fig. 9. S-parameters of different antenna structure.

This is because the dimension of the stub only affect the length of θ_3 in Fig. 3(a). However, it's important to note that the stub length not only affects the location of the hybrid mode but also has an impact on impedance matching. Consequently, a trade-off between impedance matching and mutual coupling level may arise when dealing with multiple hybrid modes.

B. Quadruplex Slot Antenna

Fig. 6 shows the proposed quadruplex antenna. There are four antennas in this module, namely ant. 1, ant. 2, ant. 3, and ant. 4, which are corresponding to the antennas excited to port 1, port 2, port 3, and port 4, respectively. A filtering antenna architecture is adopted for the ant. 3 and ant. 4 to extend their impedance bandwidths.

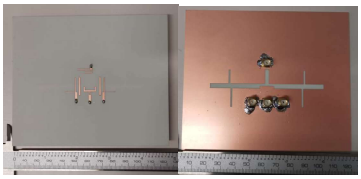

Fig. 10. Photograph of the fabricated prototype.

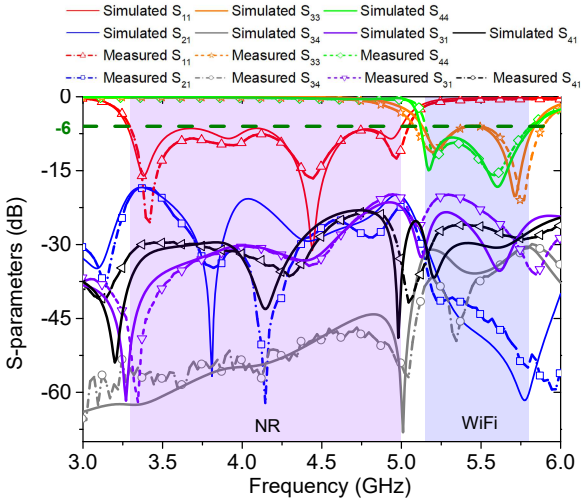

Fig. 11. Simulated and measured performance for the quadruplex antenna.

Fig. 7 presents the coupling topologies for both WiFi antennas. For the first WiFi antenna excited by port 3, in order to excite the even mode of the slot solely, a symmetric feeding structure is adopted. The symmetric feeding scheme will then activate the even mode resonance of the slot radiator to form a second-order filtering response [26]. For the second WiFi antenna related to port 4, an asymmetric feeding scheme. Port 4 is tapped to a half-wavelength resonator. This resonance will then excite the odd mode resonance of the slot through the microstrip-line-to-slot transition.

Fig. 8 shows the evolution of the proposed wideband slot antennas (Ant. 1 and Ant. 2), wherein current vectors at different resonances are also plotted with Port 2 (P2) excited. Fig. 9 illustrates the *S*-parameters of different designs. First, two additional quarter wavelength resonators are loaded on the slot as illustrated in Fig. 8 (a). Such a resonator-loading slot structure can also realize a hybrid resonant mode which has been analyzed [27]. The resonator-slotline hybrid mode (RSHM) at 4.2 GHz are also inherently decoupled, exhibiting a null in the transmission coefficient between two ports as shown in Fig. 9. Then, to further improve the bandwidth, multiple stubs are added to the slot as shown in Fig. 8 (b) and (c). With the loading of one pair of stubs, a new higher-order mode is shifted down to the frequency of interest (red lines in Fig. 9) [28], [29]. The current distribution at this resonance (4.5 GHz) is plotted in Fig. 8 (b). By introducing two more stubs, an additional resonance is observed, as illustrated by the black lines in Fig. 9. The current vector plot for this new mode in Fig 8 (c) also indicates its status as another higher-order mode. Finally, a wideband response with four resonances in the operating band is achieved.

III. Experimental Verification and Discussions

To verify the concept, a prototype of the proposed quadruplex antenna is fabricated and tested. Fig. 10 shows the photograph of the fabricated prototype. The final simulated and measured responses for the optimized quadruplex slot antenna are presented in Fig. 11. There

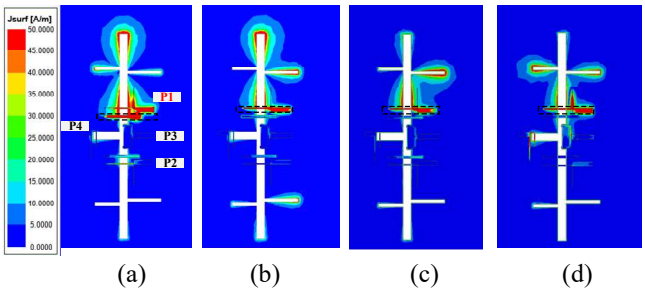

Fig. 12. Current distributions at different frequencies when ant. 1 is excited. (a) 3.4 GHz. (b) 3.9GHz. (c) 4.4GHz. (d) 4.9GHz.

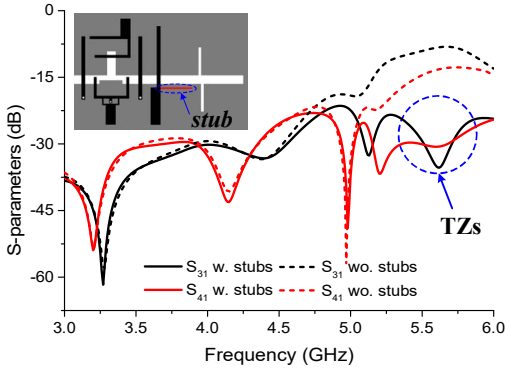

Fig. 13. Simulated and measured OBD performance.

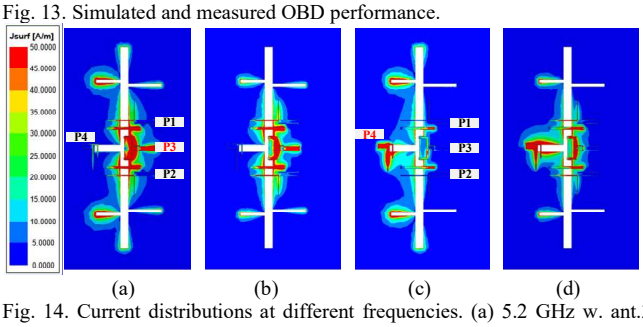

Fig. 14. Current distributions at different frequencies. (a) 5.2 GHz w. ant.3 excited. (b) 5.8 GHz w. ant.3 excited. (c) 5.2GHz w. ant.4 excited. (d) 5.8 GHz w. ant.4 excited.

are four ports in this module. These antennas can be divided into two 2×2 MIMO arrays. Then the decoupling problems regarding this structure can be categorized into two parts: in-band decoupling and out-of-band decoupling.

A. In-band performance

The operating band for ant. 1 and ant. 2 with S_{11} < -6 dB is from 3.295 GHz - 5.045 GHz. The measured isolation between two NR antennas is higher than 18.5 dB from 3.3 GHz to 5 GHz. Four hybrid modes are excited for each NR antenna as shown in Fig. 11. These modes all have their corresponding twin TZs near their resonance frequencies, although some of these TZs may not have very deep nulls on the curves because of their low quality factors. These TZs greatly improve the isolation during operating band.

The measured -6 dB bandwidth for ant. 3 and ant. 4 are 5.08GHz–5.88GHz and 5.145GHz-5.81GHz, respectively. Within the operating band of ant. 3 and ant. 4, the measured isolation between ant. 3 and ant. 4 is higher than 30.4 dB. The high isolation can be attributed to the fact that even (excited by ant. 3) and odd (excited by ant. 4) modes are orthogonal with each other [17], [18].

B. Out-of-band performance

Measurements show that the isolation between the WiFi antennas and NR antennas exceeds 19.8 dB across the entire band of interest. Consider the NR frequency range first (3.3 GHz-5 GHz). The first factor that improves the adjacent-band decoupling is the MSHM

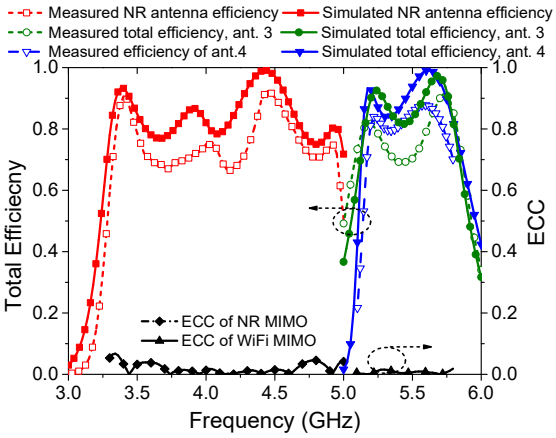

Fig. 15. Simulated and measured radiation performance of the quadruplex antenna.

structure. These hybrid modes show weak current density in the region between two NR ports as shown in Fig. 12, which shows the field distributions when port 1 is excited. These current distributions reveal that when ant. 1 is activated, the current density at the other three ports is very weak for all four frequency points, which means that the signal injected into port 1 can hardly be coupled to other ports.

For all the frequency points the current always concentrates at the upper part of the module as shown in Fig. 12. This characteristic greatly improved the isolation performance at the low frequency range. At the low-frequency band, the current is blocked by the loading resonator as shown in Fig. 12(a). For the frequency range dominated by the MSHMs, the current boundary is the feedline stub as shown in Fig 11 (b), (c), and (d). Consequently, when two WiFi ports are positioned between two NR ports, the WiFi ports become effectively isolated from the NR ports. This effect greatly improves the isolation between these two channels in the frequency range of 3.3 GHz to 5 GHz.

Another technique that enhances adjacent-band isolation is the use of filtering antenna architecture for WiFi antennas. The filtering structures of the WiFi antennas decrease the interference between NR and WiFi antennas in the frequency range of NR bands.

The out-of-band decoupling in the frequency range from 5GHz-5.8GHz is mainly realized by two open-end stubs on the feedline of the NR ports. The stubs can introduce TZs at the frequency point where their total lengths are about a quarter wavelength at both the curves of S_{31} and S_{41} as shown in Fig. 13. At these points, the open ends of the stubs transform into short ends, resulting in virtual shorting of port 1 and port 2 to ground. Consequently, interference from the other two ports is suppressed [30]. With these stubs, the isolation between the NR and WiFi antennas can be improved from 8 dB at about 5.65 GHz to 24 dB.

Regarding the higher decoupling band from 5 GHz to 5.8 GHz, current distributions are depicted in Fig. 14. Fig. 14 (a) and (b) show the current distributions when port 3 is excited. Port 3 activates the even mode of the slot with very weak current density at the central slot stub. Owning to the decoupling techniques used, all the other three ports show weak current density. Fig. 14 (c) and (d) show the current distribution when port 4 is solely excited. Port 4 activates the odd mode of the slot, resulting in a strong current density at the center stub of the slot. The orthogonality between the odd and even modes ensures good isolation between port 3 and port 4. The decoupling techniques adopted prevent the signal from port 4 transmitting to port 1 and port 2. Consequently, all the other three ports show weak current density.

C. Radiation performance

The radiation performance of the fabricated prototype is measured in an anechoic chamber with results presented in Fig. 15. As ant. 1 and ant. 2 are identical, only three antennas are measured. It should be

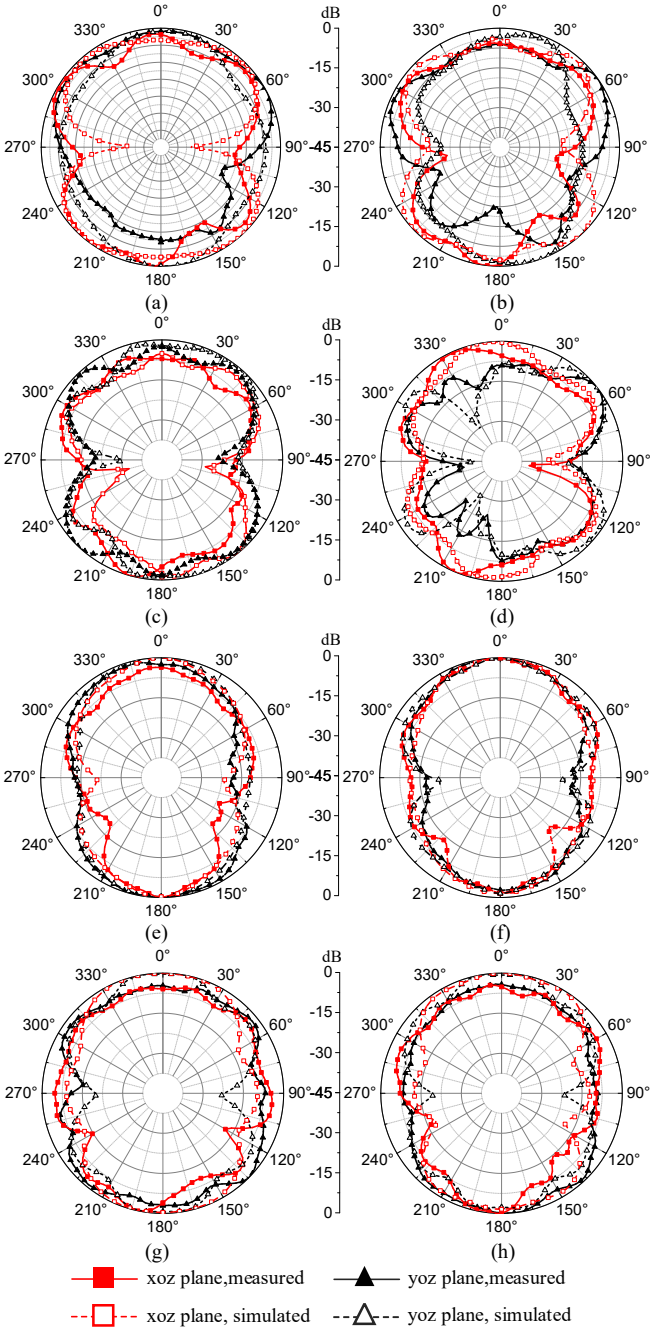

Fig. 16. Simulated and measured radiation performance of the quadruplex antenna. (a) 3.4 GHz w. ant.1 excited. (b) 3.9 GHz w. ant.1 excited. (c) 4.4 GHz w. ant.1 excited. (d) 4.9 GHz w. ant.1 excited. (e) 5.2 GHz w. ant.3 excited. (f) 5.8 GHz w. ant.3 excited. (g) 5.2GHz w. ant.4 excited. (h) 5.8 GHz w. ant.4 excited.

noted that in this process, the other three ports are all 50-Ohm terminated when one antenna is tested. The measured total efficiency for the NR antennas is higher than 56%. For the NR MIMO, the envelope correlation coefficient (ECC) value calculated from radiation patterns is lower than 0.07. For the WiFi antennas, the total efficiencies for the ant. 3 and ant. 4 are better than 69% and 53%, respectively. The ECC for the WiFi MIMO array is lower than 0.02. The measured efficiencies are generally lower than the corresponding simulations, which can be attributed to the fabrication and measurement errors and unwanted leakage from the cable during the

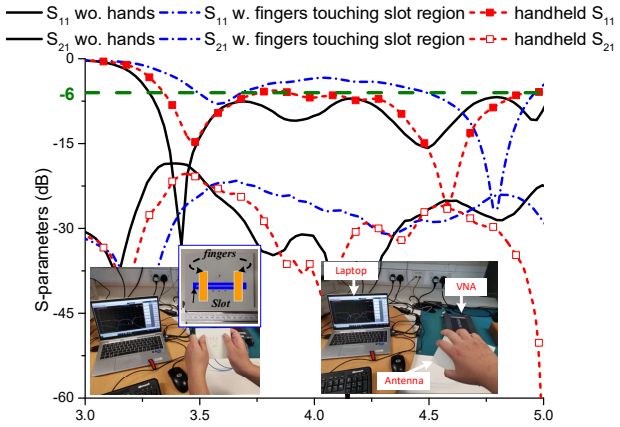

Fig. 17. Measured antenna performance in different environment.

TABLE I
PERFORMANCE COMPARISON BETWEEN THIS WORK AND OTHER PRESENTED WORKS

Ref.	FR	IBD/ OBD	NoP	BW	Iso. (dB)	Size (S×H)
[13]	1	IBD	4	41%	13	$0.77\lambda_g^2\times0.14\lambda_g$
[14]	1	IBD	3	5.7%	11	$0.14\lambda_g^2\times0.056\lambda_g$
[16]	1	IBD	3	7%, 8%, 4.5%	24, 30, 30	$0.32\lambda_g^2\times0.077\lambda_g$
[17]	1	IBD	2	6%	23	$0.2\lambda_g^2\times0.09\lambda_g$
[19]	1.97, 1.5	OBD	3	19%, 17.8%, 9.5%	28.9, 19.1, 19.3	$0.19\lambda_g^2\times0.016\lambda_g$
[22]	2.24	OBD	2	4%, 12%	26	$0.16\lambda_g^2\times0.015\lambda_g$
[23]	1.05	OBD	2	<10%	22	$0.1\lambda_g^2\times0.012\lambda$
[24]	1.18, 1.1, 1.07	OBD	4	5%, 3%, 2.8%, 4.4%	28, 29, 31.7	$1.36\lambda_g^2\times0.034\lambda_g$
This work	1.03	Both	4	41.8%, 12%	18.5, 19.8, 30	$0.93\lambda_g^2\times0.016\lambda_g$

Notes: FR: Frequency Ratio; NoP: Number of ports; BW: Bandwidth; Iso.: Isolation; S×H: Surface area × height; λg: Guided wavelength in the substrate.

radiation performance measurement, which is very common for slot antenna measurement with finite ground plane.

The normalized radiation patterns 2-D cuts at *xoz* and *yoz* planes are measured with results provided in Fig. 16. Good omnidirectional radiation patterns can be observed for all the antennas. The small ripples in the radiation patterns are mostly due to the scattering effect of the cable and connectors used in the measurement process. This phenomenon is commonly observed in many other MIMO antennas with slot structures.

D. Environmental Sensitivity

As it is widely acknowledged that the slot structure is very sensitive to the environment. To investigate the robustness of the proposed structure in different environmental conditions, some real-time measurements are carried out in this section.

From the results presented in Fig. 17, it can be seen that in a handheld scenario, the proposed bandstop radiative structure works well, maintaining a minimum isolation of 20 dB and reflection coefficient lower than -5.6 dB across the entire NR bands. However, due to the dielectric loading effect of the human tissue, a slight frequency shift is observed. This shift becomes more significant when the hands approach closer to the antenna. In an extreme scenario where

human fingers make contact with the dielectric substrate at the backside of the slot region, the in-band responses of the antennas are strongly distorted. The in-band S_{11} increases to -3.3 dB and more significant frequency shift is observed.

According to these results, it is found that this module is not well-suited for portable devices. Instead, it is very useful for applications such as routers and customer premise equipment products, which are typically mounted on a platform.

E. Comparison and Discussion

The performance of the proposed quadruplex is compared with state-of-the-art multiplex antenna designs in the literature and summarized in Table I. Notably, this proposed design addresses both in-band and out-of-band decoupling problems for the first time. Additionally, it achieves out-of-band operation with a frequency ratio of only 1.03, which is the smallest to the best of the authors' knowledge when compared to other presented multiplex-antennas. Although some designs also achieve multiplex operation at different frequency bands, they are only verified with relatively larger frequency ratios and narrow bandwidths. Regarding bandwidth, the proposed structure demonstrates a much wider frequency bandwidth than other planar designs. The general isolation level of 18.5 dB is also adequate for most terminal applications. In summary, the proposed design achieves highly competitive performance regarding bandwidth, isolation, and size.

IV. Conclusion

In this paper, a quadruplex slot antenna has been introduced. The module is composed of two MIMO arrays. Two antennas operating over 3.3 GHz-5 GHz are designed for 5G NR MIMO application. The other two antennas target the 5-GHz WiFi application. The proposed module has achieved four isolated channels in a very compact form factor. Multiple decoupling techniques have been utilized in this work, including hybrid mode theory, even-odd mode theory, filtering antenna architecture, and band-rejective open-end stubs. Especially, a new bandstop radiative concept has been presented for achieving wideband decoupling. For the first time, an antenna module addressing both wideband in-band duplex and small frequency ratio out-of-band duplex has been achieved. With this module, two wireless standards have been covered in a very compact structure, showing promising application prospects for modern terminal communication systems.

References

[1] Y.-M. Zhang *et al.*, "A transmission-line-based decoupling method for MIMO antenna arrays," *IEEE Transactions on Antennas and Propagation,* vol. 67, no. 5, pp. 3117-3131, 2019.

[2] J. Andersen, and H. Rasmussen, "Decoupling and descattering networks for antennas," *IEEE Transactions on Antennas and Propagation,* vol. 24, no. 6, pp. 841-846, November 1976.

[3] Y.-F. Cheng *et al.*, "Reduction of mutual coupling between patch antennas using a polarization-conversion isolator," *IEEE Antennas and Wireless Propagation Letters,* vol. 16, pp. 1257-1260, 2017.

[4] M. Li, B. G. Zhong, and S. W. Cheung, "Isolation enhancement for mimo patch antennas using near-field resonators as coupling-mode transducers," *IEEE Transactions on Antennas and Propagation,* vol. 67, no. 2, pp. 755-764, 2019.

[5] A. Diallo *et al.*, "Study and reduction of the mutual coupling between two mobile phone pifas operating in the dcs1800 and umts bands," *IEEE Transactions on Antennas and Propagation,* vol. 54, no. 11, pp. 3063-3074, 2006.

[6] M. M. Nikolic *et al.*, "Microstrip antennas with suppressed radiation in horizontal directions and reduced coupling," *IEEE Transactions on Antennas and Propagation,* vol. 53, no. 11, pp. 3469-3476, 2005.

[7] A. Askarian, J. Yao, Z. Lu, and K. Wu, "Surface-wave control technique for mutual coupling mitigation in array antenna," *IEEE Microwave and Wireless Components Letters,* vol. 32, no. 6, pp. 623-626, 2022.

[8] H. Lin *et al.*, "Weak-field-based self-decoupling patch antennas," *IEEE Transactions on Antennas and Propagation,* vol. 68, no. 6, pp. 4208-4217, 2020.

[9] J.-F. Qian *et al.*, "Mutual coupling suppression between two closely placed patch antennas using higher order modes," *IEEE Transactions on Antennas and Propagation*, pp. 1-1, 2023.

[10] K. Saurav *et al.*, "A three-port polarization and pattern diversity ring antenna," *IEEE Antennas and Wireless Propagation Letters,* vol. 17, no. 7, pp. 1324-1328, 2018.

[11] Y. He, and Y. Li, "Compact co-linearly polarized microstrip antenna with fence-strip resonator loading for in-band full-duplex systems," *IEEE Transactions on Antennas and Propagation,* vol. 69, no. 11, pp. 7125-7133, 2021.

[12] D. Inserra, and G. Wen, "Dual orthogonal port stacked patch antenna with vertical pins for simultaneous transmit and receive application," *IEEE Transactions on Antennas and Propagation,* vol. 69, no. 12, pp. 8908-8913, 2021.

[13] K.-L. Wong *et al.*, "Four-port wideband annular-ring patch antenna generating four decoupled waves for 5G multi-input–multi-output access points," *IEEE Transactions on Antennas and Propagation,* vol. 69, no. 5, pp. 2946-2951, 2021.

[14] B. Yang *et al.*, "Tri-port antenna with shared radiator and self-decoupling characteristic for 5G smartphone application," *IEEE Transactions on Antennas and Propagation,* vol. 70, no. 6, pp. 4836-4841, 2022.

[15] Y. Zhang *et al.*, "A compact dual-mode metamaterial-based loop antenna for pattern diversity," *IEEE Antennas and Wireless Propagation Letters,* vol. 14, pp. 394-397, 2015.

[16] X. Gao *et al.*, "Low-profile planar tripolarization antenna for wlan communications," *IEEE Antennas and Wireless Propagation Letters,* vol. 9, pp. 83-86, 2010.

[17] A. Zhang *et al.*, "High-isolated coupling-grounded patch antenna pair with shared radiator for the application of 5g mobile terminals," *IEEE Transactions on Antennas and Propagation,* vol. 70, no. 9, pp. 7896-7904, 2022.

[18] H. Xu, *et al.*, "A Highly Integrated MIMO Antenna Unit: Differential/Common Mode Design," in IEEE Transactions on Antennas and Propagation, vol. 67, no. 11, pp. 6724-6734, Nov. 2019.

[19] P. Cheong *et al.*, "A highly integrated antenna-triplexer with simultaneous three-port isolations based on multi-mode excitation," *IEEE Transactions on Antennas and Propagation,* vol. 63, no. 1, pp. 363-368, 2015.

[20] K. R. Boyle *et al.*, "A dual-fed, self-diplexing PIFA and rf front-end," *IEEE Transactions on Antennas and Propagation,* vol. 55, no. 2, pp. 373-382, 2007.

[21] W. Chujo *et al.*, "A two-layer self-diplexing antenna using a circularly polarized ring patch antenna," Antennas and Propagation Society Symposium 1991 Digest, London, ON, Canada, 1991, pp. 338-341 vol.1.

[22] Y.-C. Lu, and Y.-C. Lin, "A mode-based design method for dual-band and self-diplexing antennas using double t-stubs loaded aperture," *IEEE Transactions on Antennas and Propagation,* vol. 60, no. 12, pp. 5596-5603, 2012.

[23] A. Boukarkar *et al.*, "A tunable dual-fed self-diplexing patch antenna," *IEEE Transactions on Antennas and Propagation,* vol. 65, no. 6, pp. 2874-2879, 2017.

[24] K. Kumar *et al.*, "Self-quadruplexing circularly polarized SIW cavity-backed slot antennas," *IEEE Transactions on Antennas and Propagation,* vol. 68, no. 8, pp. 6419-6423, 2020.

[25] J. Lee *et al.*, "Lumped-element realization of absorptive bandstop filter with anomalously high spectral isolation," *IEEE Transactions on Microwave Theory and Techniques,* vol. 60, no. 8, pp. 2424-2430, 2012.

[26] J.-F. Qian et al., "A wide stopband filtering patch antenna and its application in mimo system," *IEEE Transactions on Antennas and Propagation*, vol. 67, no. 1, pp. 654-658, 2019.

[27] J.-F. Qian *et al.*, "Resonator-loaded multi-band microstrip slot antennas with bidirectional radiation patterns," *IEEE Transactions on Antennas and Propagation,* vol. 67, no. 10, pp. 6661-6666, 2019.

[28] H. Wang *et al.*, "Modal analysis and excitation of wideband slot antennas," *IET Microwaves, Antennas & Propagation,* vol. 11, no. 13, pp. 1887-1891, 2017.

[29] W.-J. Lu, and L. Zhu, "Wideband stub-loaded slotline antennas under multi-mode resonance operation," *IEEE Transactions on Antennas and Propagation,* vol. 63, no. 2, pp. 818-823, 2015.

[30] J.-S. Hong and M. J. Lancaster, Microstrip Filters for RF/Microwave Applications, New York, NY, USA:Wiley, 2001.